Direct observation of electric charges at solid/liquid interfaces with the pressure-wave-propagation method

Assane Ndour[1], Stéphane Holé[1], Paul Leblanc[2] and Thierry Paillat[2]

[1] Laboratoire de Physique et d'Étude des Matériaux
Sorbonne Université – ESPCI-Paris, PSL Université – CNRS
10, rue Vauquelin – 75005 Paris – France

[2] Institut PPRIME – Université de Poitiers – CNRS
Boulevard Marie et Pierre Curie – 86962 Futuroscope Chasseneuil – France

May 10, 2021

Abstract

Development of intrinsic electric charges at solid/liquid interfaces is still not fully understood and may generate large industrial damages by electrostatic discharges due to flow electrification. The pressure-wave-propagation (PWP) method is used to study solid/liquid interfaces in still and flowing conditions. Experimental results are shown with aluminum, brass, copper or pressboard in contact with demineralized water, salted water, glycerol or mineral oil. Salted water presents larger charge extent than expected. In still conditions with glycerol, copper gives more charges and pressboard has the largest charge extent. In flowing conditions, signal decrease seems attributed to physico-chemical time constant.

1   Introduction

When two materials are brought into contact, physico-chemical interface phenomena induce electric charge transfer from one material to the other. The contact between a solid and a liquid is no exception. That charge transfer progressively leads to a space charge buildup in each material, often called electrical double layer [1, 2]. And when the liquid is flowing, part of electric charges in the liquid is displaced and possibly further buildup until an electrostatic discharge is triggered. This is known as flow electrification [3, 4]. Although the understanding of physico-chemical phenomena taking place at the interface could by itself legitimate the interest of the scientific community, the hazard due to flow electrification, which is often associated with a major risk for industries [5, 6, 7], attracts many attention for obvious safety reasons [8, 9].

The characterization of flow electrification is most often studied either by monitoring the flow current, or the accumulation of charges or potential in the solid. Significant parameters influencing flow electrification have been determined, such as the nature of the solid-liquid couple [10, 11], the velocity and flow regime [12, 13, 14, 15], the electrical conductivity of the liquid [8, 16, 17], the temperature... This is well adapted for studying flowing liquids but less for studying still liquids. And little studies use direct and local measurement methods for determining intrinsic space charge buildup at solid/liquid interface [18, 19, 20, 21, 22]. These latter use either the Kerr effect, which restricts the studied liquid to transparent and electro-optic materials, or thermal diffusion, which may produce thermal convection inside the liquid.

Among space charge distribution measurement methods [23], the pressure-wave-propagation (PWP) method has been shown to be sensitive to phenomena taking place at solid/solid interfaces [24]. In this method, a unipolar pressure pulse is transmitted into the tested sample. During the propagation, the charges encountered are slightly displaced, generating in turn a measurable electric signal. Since the pressure wave displaces the charges one after another, the measured signal is an image of their distribution, time and space being connected by the velocity of sound.

In this paper, the pressure-wave-propagation method is used for testing solid/liquid interfaces both in still and flowing conditions. After a brief description of the electrical double layer phenomenon taking place at solid/liquid interfaces, a short survey of space charge distribution measurement methods is presented by indicating why the pressure-wave-propagation method is particularly well suited for studying solid/liquid interfaces. Then experimental results with various parameters are presented and discussed for highlighting the potentialities of the method before conclusion.

2 Solid/liquid interface

The physico-chemical phenomena taking place at the interface between a solid and a liquid exist with conductive or dielectric materials whatever their chemical nature. The charge transfer between the two materials in contact yields to the formation of two opposite charge regions, one in the solid and the other inside the liquid. That structure is often called the electrical double layer (EDL) [1, 2]. The very origin of these phenomena is still poorly identified and several assumptions have been proposed, such as adsorption and desorption of charge carriers, corrosion, difference in working function between solid and liquid materials [13, 25, 26, 27], ...

In 1853, Helmholtz proposed the first model of the EDL [28] by assimilating the two charged regions as the electrodes of a plane capacitor, the charge distribution being maintained at the interface only by electrostatic forces. This is known as the compact Helmholtz layer, which thickness d_0 is assumed to be of the order of the ionic radius in the liquid. Figure 1a illustrates the charge, electric field and electric potential distributions at the interface for Helmholtz model. However, the assumption of a uniform charge distribution was challenged in the early 1900s by Gouy and Chapman [29, 30]. In addition to electrostatic forces, they added diffusion to the model. Charge carriers are then distributed in the liquid from the solid interface according to a Boltzmann law [31] as shown in Figure 1b. If n is the carrier density in the liquid, n_0 the carrier density in the liquid far from the interface and $\varphi(x)$ the electric potential distribution in the liquid as a function of

depth x from the interface, one has

$$n = n_0 \exp(-q\varphi/kT) \tag{1}$$

where q is the considered carrier charge, k is the Boltzmann constant and T is the temperature. When $|q\varphi| \ll kT$, the mean depth of the charge distribution in the liquid corresponds to the Debye length δ_0 as [32]

$$\delta_0 = \sqrt{\frac{\epsilon kT}{q^2 n_0}} = \sqrt{\frac{\epsilon D_0}{\sigma}} \tag{2}$$

where ϵ is the liquid permittivity, D_0 is the liquid electric diffusivity and σ is the liquid electric conductivity. An improvement was proposed by Stern in 1924 [1]. His model is a combination of Helmholtz and Gouy-Chapman models and takes into account the size of ions. It is composed of two sub-layers inside the liquid: a compact layer at the interface and a diffuse layer farther, as illustrated in Figure 1c. The compact layer extends over a few angstroms and charges in this layer are stuck to the interface and thus are not perturbed by any liquid flow. The diffuse layer is similar to the Gouy-Chapman layer. The charges in the diffuse layer are assumed to be free to move and thus are susceptible to drift with the liquid when it flows. The limit between these two sub-layers is called the slipping plane and the potential at this limit is called ζ potential [33].

The charge distribution in the liquid does not buildup instantaneously. The time necessary for the interface to polarize and the time necessary to reach the equilibrium are two parameters that account for the EDL buildup time. The first time constant τ_{ch}, which corresponds to the appearance of charges at the interface, is directly linked to the speed of the physico-chemical reactions between the solid and the liquid, therefore depends on the nature of the reactants, their concentration and the temperature [25]. The second time constant τ_r, which corresponds to the relaxation time to get to the equilibrium, corresponds more or less to the time required for a charge to diffuse across the Debye length δ_0, one has

$$\tau_r = \frac{\delta_0^2}{D_0} = \frac{\epsilon}{\sigma}. \tag{3}$$

According to the Stern model of the EDL, the charges in the diffuse layer are free to move and thus can drift under an applied electric field or a liquid flow. This results in two electro-kinetic phenomena: the electro-osmosis and the flow electrification. In electro-osmosis, a tangential electric field applied to a liquid in contact with a solid surface, tends to move the charges of the diffuse layer. Due to viscosity, the charge displacement can drag the fluid [34, 35, 36]. In flow electrification, the liquid flow drags the charges of the diffuse layer and consequently disturbs the electrostatic state of equilibrium. This induces an electric current in the liquid, called the flow current. To compensate for the charges transported by the flow, physico-chemical reactions at the interface attempt to establish a new state of equilibrium (dynamic equilibrium) by generating new charges [37, 38]. During the flow, the solid also accumulates electrical charges. Therefore, if the solid in contact with the liquid is a dielectric or is electrically isolated from earth, the accumulation of charges can result in a sufficiently high potential to trigger uncontrolled electrostatic discharges and cause hazards.

3 Measurement method

3.1 Choice of the measurement method

The main measurement methods to study electric phenomena arising at solid/liquid interfaces rely on electrostatics. Charges in the diffuse layer are dragged by the liquid flow and are measured in turn by charge counting, current measurement in the fluid flow, potential variation, or generated current measurement [39, 40, 41, 42]. These measurement methods are very sensitive but work only in dynamic equilibrium, so they do not give access to the complete image of the interface phenomena.

Measurement in static equilibrium is well known in the case of dielectrics under voltage and 3 main measurement methods [23] are often used to determine the space charge distribution (see Figure 2). They all consist in a slight perturbation of the local electro-mechanical equilibrium in the tested material.

In the thermal method [43] illustrated in Figure 2a, heat is transmitted to the tested insulating structure (sample) and expands the material during heat diffusion, thus displacing the charges encountered. This charge displacement gives rise to a measurable electric signal. The thermal method is sensitive, well adapted to interface measurements and has already been tested to characterize solid/liquid interfaces [44]. However, heat diffusion generates by nature a signal quite complex to analyze and is very sensitive to noise reducing as a consequence the confidence in the interpretation of the data.

In the pressure-wave-propagation (PWP) method [45, 46] illustrated in Figure 2b, a pressure wave is transmitted to the sample and then propagates inside. During the propagation, the charge encountered are slightly displaced one after another, resulting in a current at the image of the charge distribution when the pressure wave has a pulse shape, space and time being simply connected by the velocity of sound. Therefore, inverse convolution calculations are not mandatory to analyze the data and confidence in the interpretation is greatly improved.

In the pulsed-electro-acoustic (PEA) method [47] illustrated in Figure 2c, the perturbation consists in applying a fast voltage variation, generally a pulse, to the sample. The resulting variation of electrostatic force acting on charges inside the sample generates elastic waves that can be measured by an ultrasonic sensor coupled to the sample. The obtained signal is also an image of the charge distribution since the elastic waves take more time to reach the sensor when the charges at the origin of these waves are farther from the sensor.

Though the signal is very simple to analyze in the case of PWP and PEA methods, the signal produced by the interface is strongly perturbed by the fast voltage variation in the case of the PEA method. Indeed, the fast voltage variation applied to the sample induces charges at the interfaces which generate a signal that mixes with the one produced by interface phenomena. Finally, it is more convenient to use the pressure-wave-propagation method since interface phenomena are not masked and since signals are more easy to analyze.

3.2 Setup description

A specific measurement setup, sketched in Figure 3, has been made for this study. Pressure waves are generated in an aluminum wave-guide by an ultrasonic generator [48, 49] delivering unipolar pressure

pulses of about $P_0 = 10\,\text{MPa}$ in amplitude and $\tau = 40\,\text{ns}$ in duration at 50-Hz rate. This ultrasonic generator, studied in details in [48] and described for space charge measurements for instance in [49], is composed of a 200-μm-thick 15-mm-diameter piezoelectric ceramic which is stuck on one side to the aluminum wave-guide and on the other side to a brass backing. A piezoelectric ceramic Pz24 from Meggitt is used since it has a large g piezoelectric constant which is a good compromise for fast voltage variation and large mechanical response. This sandwich structure allows unipolar pressure pulses to be generated with the application of voltage steps, here of about 200-V amplitude. Considering the transmission from the wave-guide to the liquid, the fluid displacement u due to a pressure pulse is thus of the order of

$$u = \frac{2\tau P_0}{Z_\ell + Z_g} \approx 40\,\text{nm} \tag{4}$$

where Z_ℓ and Z_g are respectively the acoustic impedance of the liquid (about 1.5 MRayl for water) and of the wave-guide (of the order of 17.2 MRayl for aluminum). This displacement can be considered negligible compared to the tested liquid thickness.

In the setup, the aluminum wave-guide is not coated, it is thus in direct contact with the liquid to form the front interface. On the opposite side, the back interface, a brass electrode is used to measure the electric signal induced by the pressure wave which is first amplified by an Analog Module 322-12-50 amplifier (60 dB, 50 Ω input and output impedance) and then digitize by a Tektronic DPO 3034 scope which averages 512 acquisitions for improving signal-to-noise ratio. All measured signals shown thereafter are raw signals, directly obtained from the scope without additional signal processing. The back electrode can hold various materials to vary the nature of the back interface. Therefore the structure of the sample is composed of two solid/liquid interfaces, one with aluminum at the front side and one with various materials at the back side. It is worth noting that, due to the pressure wave reflection at the back interface, the amplitude of the signal at the back interface is scaled by

$$\frac{2Z_\ell}{Z_b + Z_\ell} \tag{5}$$

where Z_b is the acoustic impedance of the material at the back interface, which is supposed sufficiently thick to avoid standing waves. Between the interfaces, the liquid can remain immobile or can flow at various speeds thanks to a peristaltic pump. Moreover, as any measurement system, the setup can be impacted by various spurious effects. Since the PWP method relies on an acousto-electric coupling, electric shielding, electric contacts and acquisition averaging is important for noise reduction, and pressure generation and mechanical properties of the various materials in the tested structure must be taken into account.

4 Results and discussion

4.1 Typical signals

A typical signal is shown in Figure 4 with and without demineralized water inside the measurement setup. When no liquid is inside the measurement setup, only noise is detected and the signal remains close to the base line. However, when water enters the setup, two distinct features appear clearly in the signal, one

at 4.73 μs and another at 5.86 μs. The first feature at 4.73 μs corresponds to the entrance of the pressure pulse in the liquid thus to the signal generated at the front interface. The 4.73-μs delay corresponds to the transit time of the pressure wave inside the 3-cm-thick aluminum wave-guide. The second feature at 5.86 μs corresponds to the exit of the pressure pulse from the liquid, thus to the signal at the back interface. The time delay between the two interface signals corresponds to the transit time of the pressure wave in the liquid, here about 1.8 mm of water. The interface signal is mainly bipolar, one polarity for the charges in each side of the interface. The signal polarity is positive in the solids (here aluminum at front side and brass at back side) and negative in the liquid. This is coherent since most cases report liquids negatively charged and solids positively charged, for instance between glycerol and steel in [50]. The signal duration at mid-amplitude depends both on the duration of the pressure pulse and on the spatial distribution of the charges. As the pressure pulse is of the order of 40-ns duration, it corresponds in water to a spatial resolution of 60 μm. Therefore charges extending over less than 60 μm are measured as a whole and it is not possible to estimate their extent. In that case, the signal exhibits a peak which duration is similar to the pressure pulse duration and which amplitude is proportional to the whole charge quantity. On the contrary, if the signal lasts more than 40 ns, the charge extent can be estimated thanks to the velocity of sound in the liquid. In that case, the signal exhibits a peak or a plateau which duration is larger than the pressure pulse duration and which amplitude corresponds to the charge quantity over the pressure pulse extent. Roughly speaking, the signal duration lasts the pressure pulse duration plus the charge extent divided by sound velocity. Notice that ripples after the bipolar signal at the entrance are due to a small resonance in the measurement setup. At the back side however, charges are detected as soon as about 150 μm from the interface.

When the thickness of the liquid varies, the amplitude of the signal does the same, as shown in Figure 5 for glycerol. The plot of the peak-to-peak signal amplitude at each interface as a function of the liquid thickness shows a similar trend for both interfaces. This is confirmed by the ratio between the two amplitudes (see the inset in Figure 5) which is more or less constant whatever the liquid thickness, indicating that the measurement setup sensitivity is inversely proportional to the liquid thickness, thus to the sample capacitance, and that attenuation of the pressure waves in the liquid can be considered as negligible in the experiments presented hereafter.

With salted water (1.25% in weight content), one clearly sees in Figure 6a the evolution of the signal with time at the two interfaces. In this figure, signals have been delayed by 50 ns from one another to show more clearly the evolution. The original signals start exactly at the same position on the time axis. The behavior is different as well as the distribution for the two interfaces. The peak amplitude corrected from the base line of these signals (see Figure 6b) indicates the stabilization of the charge distribution at the interface which depends on the dynamics of the chemical reactions and physico-chemical phenomena taking place at the interfaces and on the diffusion of charges in the liquid. For comparison between materials, thereafter we have waited sufficient time to reach equilibrium. Notice that charges seem to extend over a much larger depth at the back side than when using demineralized water though mobile carriers should have been more concentrated owing to salt and thus the Debye length should be smaller according to (2). This seems contradictory but has been already observed in highly concentrated electrolytes [51], indicating that much work remains to be done to understand completely physico-chemical phenomena taking place at liquid/solid interfaces. A possible explanation, which needs however further studies, could be that charge concentration at the interface had reached its maximum and thus had no other choice than extending inside

the liquid.

4.2   Glycerol with various solids

Figure 7 shows measurement with various solid materials at the back electrode in contact with glycerol. As the setup must be unmounted and remounted to change the back material which has various thicknesses, the overall sample thickness little varies from one measurement to another. Therefore, the back side signal is not exactly at the same position in the various measurements shown in Figure 7. Taking advantage of the aluminum wave-guide at front side for all samples and assuming no influence of the back side material on the front side signal, it is possible to normalize all signals by the front side signal amplitude for appropriate comparison. Moreover, it is worth recalling that the amplitude of the signal at the back interface must be scaled according to the acoustic impedance of the material at back side as (5).

Figure 8 reports the corrected peak-to-peak amplitude at the back side normalized with the one at the front side as well as the equivalent extent of the signal in the liquid at back side as a function of materials. Error bars are calculated from 3 measurements. The reproducibility of the signal is sufficient to imply the significance of the different behaviors between materials. It can be seen that pressboard shows the lowest level of charges compared to the other tested materials and the largest charge extent inside the liquid. This can be attributed to the porosity of pressboard which implies a more fuzzy interface. However, brass presents a quite large charge extent as well indicating, for instance, non uniform liquid properties at the interface due to chemical effects between the liquid and the solid that slightly diffuses in the liquid from the interface.

4.3   Various insulating liquids

Specific dielectric liquids are used in high voltage applications for insulating purpose. Mineral oil with various content of ALOA 218B for varying conductivity has been tested. Compared to glycerol, no signal was detected at front and back interfaces. To understand the absence of interface signal, dielectric measurements have been carried out on the various liquids and are reported in Table 1. It can be noticed that all mineral oil samples (min-x) present a much lower permittivity and conductivity than the tested glycerol samples (gly-x).

The time constant τ_r of samples min-b, min-c and min-d approaches the time between each acquisition which is of 20 ms (50-Hz rate). But as samples min-a and gly-a have similar time constant τ_r, the repetition rate of the measurement may not have any influence. More probably, the sensitivity of the measurement setup depends on the overall capacitance of the tested sample as already assumed from Figure 5b since it is inversely proportional to the sample thickness. Therefore, if the permittivity of the liquid is greatly reduced, the sample capacitance is greatly reduced as well, so the setup sensitivity should also be greatly reduced. To test that assumption, the gap between electrodes has been reduced in order to increase the sample capacitance and the number of averaged acquisitions has been increased to improve sensitivity. Results are reported in Figure 9 and shows that the signal-to-noise ratio is improved by reducing the sample thickness as well as by increasing the averaged acquisition number. When using 512 averaged acquisitions, the interface signal (here at the front side) begins to be detected with 0.5-mm-thick liquid. When using

10024 averaged acquisitions (with Tektronix MSO 54 scope), the signal is already detected for 2-mm-thick liquid. The factor 4 between 2-mm thickness and 0.5-mm thickness is coherent with the signal-to-noise ratio improvement by 4.4 when averaging 10024 acquisitions instead of 512. This clearly indicates that sensitivity is more likely to blame than the time constant if the signal were not detected at first glance. This experiment also demonstrates that the sensitivity of measurement setup directly depends on the sample capacitance.

4.4 Flowing fluid

A peristaltic pump was used to circulate glycerol at various speeds inside the measurement setup. The liquid thickness is 1.5 mm. The peak-to-peak amplitude of the signal at front and back interfaces are reported in Figure 10. The amplitude of the signal reduces with the liquid flow rate. Indeed, if the liquid is flowing, part of the charges in the diffuse layer leaves the measurement area and thus less charges are detected. There can be various origins of the decrease of the signal amplitude. For instance, it takes time to rebuild the diffusion layer and it also takes time to provide charges at the solid/liquid interface. A simplified electrical model can be proposed to evaluate the order of magnitude of the various phenomena observed, as shown in Figure 11. It can be assumed that the physico-chemical phenomena taking place at the interface produce a voltage V_i. Then, the charges generated accumulate firstly in the compact layer, which can be characterized as a capacitor C_c, and secondly in the diffuse layer, which can be characterized as a capacitor C_d. As the flow Q directly removes charges from the diffuse layer, it can be modeled by a resistor R_{flow} which volume value is $R_{flow} = 1/(QC_d)$. The linear fits of the signal amplitude in millivolt in Figure 10 with Q expressed in milliliter per second are

$$
\begin{cases}
10.45 - 0.13\,Q & \text{At front side} \\
3.12 - 0.03\,Q & \text{At back side}
\end{cases}
\tag{6}
$$

Because measurements were carried out at dynamic equilibrium, there was no longer time dependence and the simple model shown in Figure 11 can be reduced to a simple resistor bridge comprising R_c, R_d and R_{flow}. As a consequence, the signal amplitude, which is proportional to the charges in the liquid and thus to the voltage across C_d, is also proportional to

$$
\frac{R_{flow}}{R_c + R_d + R_{flow}}\,V_i = \frac{1}{1 + (R_c + R_d)\,QC_d}\,V_i.
\tag{7}
$$

The amplitude variation of the signal being relatively small compared to its amplitude (see Figure 10), a first order development can be made so that (7) becomes

$$
V_i - (R_c + R_d)C_d V_i\,Q.
\tag{8}
$$

The identification between (6) and (8) leads to

$$
\begin{cases}
(R_c + R_d)\,C_d \approx 12.4\,\text{s/L} & \text{At front side} \\
(R_c + R_d)\,C_d \approx 9.6\,\text{s/L} & \text{At back side}
\end{cases}
\tag{9}
$$

These time constants depend on the volume being taken into account. When considering the liquid volume

under test, which is about 84.4 μL, one obtains 1.05 ms at front side and 0.81 ms at back side. However, charges are not generated only at the interfaces of the tested volume, but at all interfaces of the measurement setup, pipes and tank. Therefore, if charges leave the tested area by the flow, others can enter this same area from the flow. A much larger volume could be then considered in (9) resulting in much larger time constants. Also, the liquid can flow in a non uniform way in the measurement setup. If Q were smaller in the tested area, this would also result in an increase of the time constant in (9). The time constants calculated with 84.4 μL can thus be considered as a lower limit and, since they are already much larger than τ_r for glycerol, the signal decrease observed in Figure 10 could be assumed originating from the dynamic of charge appearance at the interfaces and thus connected to the time constant τ_{ch}.

5   Conclusion

It is shown that using the pressure-wave-propagation method with a piezoelectric unipolar pressure pulse generator, it is possible to obtain a sufficient signal-to-noise ratio to detect the charges intrinsically generated at the interface between a solid and a liquid. Salted water presents a larger distribution extent than deminer-alized water at the interface with brass which seems contradictory with Stern model. Among copper, brass, aluminum and pressboard in contact with glycerol, copper presents the larger charge amplitude and press-board presents the larger charge extent. The obtained signals are proportional to the sample capacitance, so appropriate sample geometry and averaged acquisition number should be chosen, specifically for low permittivity liquids such as mineral oil. Since the signal is an image of the charge distribution throughout the sample, all interfaces can be analyzed independently. And because acquisitions are relatively rapid, still and flowing measurement conditions can be studied with the same measurement setup. With glycerol, the signal decrease as a function of flow points to a time constant much larger than the diffusion time constant which could be attributed to a physico-chemical time constant instead. As the pressure-wave-propagation method directly probes the charges by their displacement at the studied interfaces, it does not rely on an electrical model of the interface to exploit the measurements. That makes it possible to study more eas-ily and more rapidly solid/liquid interfaces presenting safety risks for industrial applications or behaving non-conventionally to elucidate unknown mechanisms. Though already helpful for qualitative studies, fur-ther work has to be done for quantitative charge evaluation at the interfaces, for instance by a calibration procedure.

References

[1] O. Stern. Zur theorie der elektrolytischen doppelschicht. *Zeitschrift für Elektrochemie und angewandte physikalische Chemie*, 30:508–516, 1924.
doi: 10.1002/bbpc.192400182.

[2] D.C. Grahame. The electrical double layer and the theory of electrocapillarity. *Chemical Reviews*, 41:441–501, 1947.
doi: 10.1021/cr60130a002.

[3] S. Wall. The history of electrokinetic phenomena. *Current Opinion in Colloid & Interface Science*, 15:119–124, 2010.
doi: 10.1016/j.cocis.2009.12.005.

[4] G. Luttgens, S. Luttgens, and W. Schubert. *Static Electricity: Understanding, Controlling, Applying*. Wiley-VCH, 2017. ISBN: 9783527341283.

[5] G Luttgens and N. Wilson. *Electrostatic Hazards*. Butterworth-Heinemann, 1997. ISBN: 9780750627825.

[6] U.S. Department of Transportation. A Review of the Flammability Hazard of Jet A Fuel Vapor in Civil Transport Aircraft Fuel Tanks. Technical report, National Technical Information Service, 1998. DOT/FAA/AR-98/26.

[7] L.G. Britton. *Avoiding Static Ignition Hazards in Chemical Operations*. Center for Chemical Process Safety concept book, 1999. ISBN: 0-8169-0800-1.

[8] A. Klinkenberg and J.L. Van Der Minne. *Electrostatics in the petroleum industry; the prevention of explosion hazards*. a royal dutch/shell research and development report. Amsterdam, 1958.

[9] I. Fofana and Y. Hadjadj. Electrical-based diagnostic techniques for assessing insulation condition in aged transformers. *Energies*, 9:679–1–26, 2016. doi: 10.3390/en9090679.

[10] E. Moreau, P. Paillat, and G. Touchard. Space charge density in dielectric and conductive liquids flowing through a glass pipe. *Journal of Electrostatics*, 51-52:448–454, 2001.
doi: https://doi.org/10.1016/S0304-3886(01)00082-1.

[11] J. Vazquez-Garcia, J. Rivenc, A. Agneray, T. Paillat, and G. Touchard. A critical approach to measure streaming current: case of fuels flowing through conductive and insulating polymer pipes. *IEEE Transactions on Industry Applications*, 41:1335–1342, 2005.
doi: 10.1109/TIA.2005.853378.

[12] A.A. Boumans. Streaming currents in turbulent flows and metal capillaries: Ii. theory (2). charge transported by the flow of liquid. *Physica*, 23:1027–1037, 1957.
doi: 10.1016/S0031-8914(57)95960-8.

[13] H.L. Walmsley and G. Woodford. The generation of electric currents by the laminar flow of dielectric liquids. *Journal of Physics D: Applied Physics*, 14:1761–1782, 1981.
doi: 10.1088/0022-3727/14/10/011.

[14] H.L. Walmsley. The generation of electric currents by the turbulent flow of dielectric liquids. i. long pipes. *Journal of Physics D: Applied Physics*, 15:1907–1934, 1982.
doi: 10.1088/0022-3727/15/10/010.

[15] J.K. Nelson. Dielectric fluids in motion. *IEEE Electrical Insulation Magazine*, 10:16–28, 1994.
doi: 10.1109/57.285419.

[16] J K Nelson and M J Lee. Electrokinetic effects in power transformers. Technical report, EPRI-EL/ER-6880, United States, 1990.

[17] T. Paillat, E. Moreau, and G. Touchard. Space charge density at the wall in the case of heptane flowing through an insulating pipe. *Journal of Electrostatics*, 53:171–182, 2001.
doi: 10.1016/S0304-3886(01)00139-5.

[18] X. Zhang, J. K. Nowocin, and M. Zahn. Evaluating the reliability and sensitivity of the kerr electro-optic field mapping measurements with high-voltage pulsed transformer oil. *Applied Physics Letters*, 103:082903, 2013.
doi: 10.1063/1.4819340.

[19] J. Shi, Q. Yang, W. Sima, L. Liao, S. Huang, and M. Zahn. Space charge dynamics investigation based on kerr electro-optic measurements and processing of ccd images. *IEEE Transactions on Dielectrics and Electrical Insulation*, 20:601–611, 2013.
doi: 10.1109/TDEI.2013.6508764.

[20] J.P. Jiang, B.X. Du, X.L. Li, B. Cui, H. Xu, M. Fu, and S. Hou. Space charge measurement of vegetable oil filled with bn nanoparticles by thermal step method. In *2016 IEEE International Conference on Dielectrics (ICD)*, volume 1, pages 176–179, 2016.
doi: 10.1109/ICD.2016.7547573.

[21] C. Cheng, Y. Wu, Y. Fan, K. Wu, K. Qian, and Y. Liu. Correlation between aging status and space charge behaviors in samples consisting of oil immersed paper and oil. In *2018 IEEE Conference on Electrical Insulation and Dielectric Phenomena (CEIDP)*, pages 614–617, 2018.
doi: 10.1109/CEIDP.2018.8544852.

[22] X. Sidambarompolé, J. Laurentie, P. Notingher, T. Paillat, P. Leblanc, G. Touchard, A. Toureille, and O. Guille. A non-destructive thermal stimulus method as a tool for studying the electrical double layer. In *2019 IEEE 20th International Conference on Dielectric Liquids (ICDL)*, pages 1–4, 2019.
doi: 10.1109/ICDL.2019.8796837.

[23] S. Holé, T. Ditchi, and J. Lewiner. Non-destructive methods for space charge distribution measurements: what are the differences? *IEEE Transactions on Dielectrics and Electrical Insulation*, 10:670–677, 2003.
doi: 10.1109/TDEI.2003.1219652.

[24] S. Holé. Contact potential measurement at metal/insulator interface. In *17th International Symposium on Electrets (ISE)*, page 51, Limerick, Ireland, 2019.
available at https://ise2019.mosaicteam.eu/wp-content/uploads/2019/09/ISE17_2019_AbstractBook.pdf.

[25] G.G. Touchard, T.W. Patzek, and C.J. Radke. A physicochemical explanation for flow electrification in low-conductivity liquids in contact with a corroding wall. *IEEE Transactions on Industry Applications*, 32:1051–1057, 1996.
doi: 10.1109/28.536865.

[26] A.P. Washabaugh and M. Zahn. A chemical reaction-based boundary condition for flow electrification. *IEEE Transactions on Dielectrics and Electrical Insulation*, 4:688–709, 1997.
doi: 10.1109/94.654576.

[27] H. Kitabayashi, K. Tsuji, and K. Itoh. A streaming electrification model based on differences of work function between solid materials and insulating oil. *Journal of Electrostatics*, 63:735–741, 2005. doi: 10.1016/j.elstat.2005.03.037.

[28] H. Helmholtz. Ueber einige gesetze der vertheilung elektrischer ströme in körperlichen leitern mit anwendung auf die thierisch-elektrischen versuche. *Annalen der Physik und Chemie*, 165:211–233, 1853. doi: 10.1002/andp.18531650603.

[29] L.G. Gouÿ. Sur la fonction électrocapilaire. *Annales de Chimie et de Physique*, 29:145–241, 1903. available at https://gallica.bnf.fr/ark:/12148/bpt6k34929r/f143.image.

[30] D.L. Chapman. A contribution to the theory of electrocapilarity. *Philosophical Magazine and Journal of Science*, 25, 6th series:475–481, 1913. available at https://archive.org/details/londonedinburg6251913lond/page/474/mode/2up.

[31] J.S. Newman. *Electrochemical systems*. Prentice Hall international series in the physical and chemical engineering sciences. Englewood Cliffs, N.J. : Prentice-Hall, 1991, 1973. ISBN: 0132487586.

[32] P. Debye and E. Hückel. Zur theorie der elektrolyte. *Physik. Z.*, 24:185–206, 1923. available at https://pdfs.semanticscholar.org/bae0/0802d46520f781221e90f4ce97aece778ca2.pdf.

[33] B.J. Kirby and E.F. Hasselbrink Jr. Zeta potential of microfluidic substrates: 1. theory, experimental techniques, and effects on separations. *Electrophoresis*, 25:187–202, 2004. doi: 10.1002/elps.200305754.

[34] F.F. Reuss. Sur un nouvel effet de l'électricité galvanique. *Mémoires de la Société Impériale des Naturalistes de Moscou*, 2:327–337, 1809. available at https://www.biodiversitylibrary.org/item/234594#page/375/mode/1up.

[35] C. L. Rice and R. Whitehead. Electrokinetic flow in a narrow cylindrical capillary. *The Journal of Physical Chemistry*, 69:4017–4024, 1965. doi: 10.1021/j100895a062.

[36] S. Levine, J.R. Marriott, G. Neale, and N. Epstein. Theory of electrokinetic flow in fine cylindrical capillaries at high zeta-potentials. *Journal of Colloid and Interface Science*, 52:136–149, 1975. doi: 10.1016/0021-9797(75)90310-0.

[37] M. El-Adawy, T. Paillat, G. Touchard, and J.M. Cabaleiro. Numerical simulation of the electrical double layer development: physicochemical model at the solid and dielectric liquid interface for laminar flow electrification phenomenon. *IEEE Transactions on Dielectrics and Electrical Insulation*, 18:1463–1475, 2011. doi: 10.1109/TDEI.2011.6032817.

[38] J. M. Cabaleiro, T. Paillat, O. Moreau, and G. Touchard. Electrical double layer's development analysis: Application to flow electrification in power transformers. *IEEE Transactions on Industry Applications*, 45:597–605, 2009. doi: 10.1109/TIA.2009.2013544.

[39] A. P. Washabaugh and M. Zahn. Flow electrification measurements of transformer insulation using a couette flow facility. *IEEE Transactions on Dielectrics and Electrical Insulation*, 3:161–181, 1996.
doi: 10.1109/94.486767.

[40] M. Zdanowski and J. Kedzia. Research on the electrostatic properties of liquid dielectric mixtures. *Journal of Electrostatics*, 65:506–510, 2007.
doi: 10.1016/j.elstat.2006.11.006.

[41] T. Paillat, G. Touchard, and Y. Bertrand. capacitive sensor to measure flow electrification and prevent electrostatic hazards. *Sensors*, 12:14315–14326, 2012.
doi: 10.3390/s121114315.

[42] P. Leblanc, T. Paillat, J.M. Cabaleiro, and G. Touchard. Flow electrification investigation under the effect of the flow parameters. *International Journal of Plasma Environmental Science and Technology*, 11:156–160, 2018.
available at http://iesj.org/IJPEST/11/2/PDF/11-02-156.pdf.

[43] R.E. Collins. Analysis of spatial distribution of charges and dipoles in electrets by a transient heating technique. *Journal of Applied Physics*, 47:4404–4408, 1976.
doi: 10.1063/1.322521.

[44] M.S. Vihacencu, Notingher P.V., T. Paillat, and S. Jarny. Flow electrification phenomenon for newtonian and non-newtonian liquids: influence of liquid conductivity, viscosity and shear stress. *IEEE Transactions on Dielectrics and Electrical Insulation*, 21:693–703, 2014.
doi: 10.1109/TDEI.2013.004423.

[45] P. Laurenceau, G. Dreyfus, and J. Lewiner. New principle for the determination of potential distributions in dielectrics. *Physical Review Letter*, 38:46–49, 1977.
doi: 10.1103/PhysRevLett.38.46.

[46] S. Holé, T. Ditchi, and J. Lewiner. Influence of divergent fields on space charge distribution measurements using elastic methods. *Physical Review B*, 61:13528–13539, 2000.
doi: 10.1103/PhysRevB.61.13528.

[47] T. Maeno, H. Kushiba, T. Takada, and C. M. Cooke. Pulsed electro-acoustic method for the measurement of volume charge in e-beam irradiated PMMA. In *Conference on electrical insulation and dielectric phenomena*, pages 389–397, Amherst NY, USA, 1985. IEEE.
doi: 10.1109/CEIDP.1985.7728298.

[48] S. Holé and J. Lewiner. Design and optimization of unipolar pressure pulse generators with a single transducer. *Journal of the Acoustical Society of America*, 104:2790–2797, 1998.
doi: 10.1121/1.423863.

[49] A. Marian, S. Holé, F. Lesur, M. Tropeano, and C.E. Bruzek. Validation of the Superconducting and Insulating Components of a High-Power HVDC Cable. *IEEE Electrical Insulation Magazine*, 34:26–36, 2018.
doi: 10.1109/MEI.2018.8246119.

[50] M. De Tinguy, T. Paillat, P. Leblanc, and G. Touchard. Critical analysis of the flow electrification measurement for a conductive solid/liquid couple. *International Journal of Plasma Environmental Science & Technology*, 14:e01001–1–9, 2020.
doi: 10.34343/ijpest.2020.14.e01001.

[51] A.M. Smith, A.A. Lee, and S. Perkin. The electrostatic screening length in concentrated electrolytes increases with concentration. *The Journal of Physical Chemistry Letters*, 7:2157–2163, 2016.
doi: 10.1021/acs.jpclett.6b00867.

List of Tables

List of Figures

Table 1: Sample properties. Samples wat-d and wat-s correspond respectively to demineralized water and salted water, gly-a and gly-b are glycerol samples and min-a to min-d are mineral oil samples containing various ALOA 318B contents.

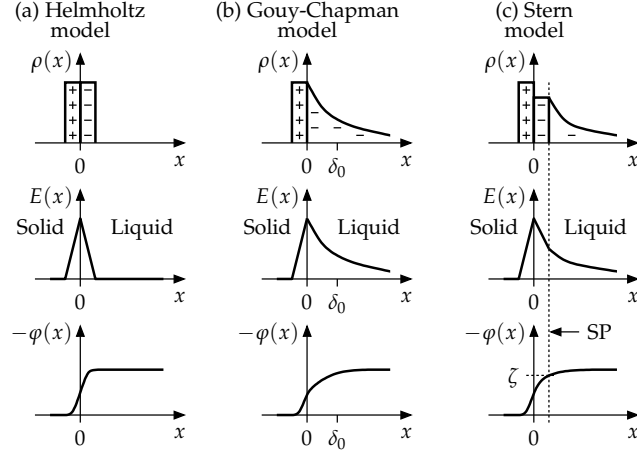| Sample	σ (nS/m)	ϵ (pF/m)	τ_r (ms)
wat-d	15 700 000	710	0.000 045 2
wat-s	1 410 000 000	620	0.000 000 44
gly-a	15 700	1 320	0.084 1
gly-b	14 000	407	0.029 1
min-a	182	20.8	0.114
min-b	7.99	21.6	2.70
min-c	7.64	21.6	2.83
min-d	3.67	21.5	5.86

Figure 1: Conventional Electrical Double Layer (EDL) models with charge distribution $\rho(x)$, electric field distribution $E(x)$ and electric potential distribution $\varphi(x)$ at a solid/liquid interface. (a) Helmholtz model, (b) Gouy-Chapman model with the mean diffusion depth δ_0 and (c) Stern model with ζ potential defined at the slipping plane (SP).
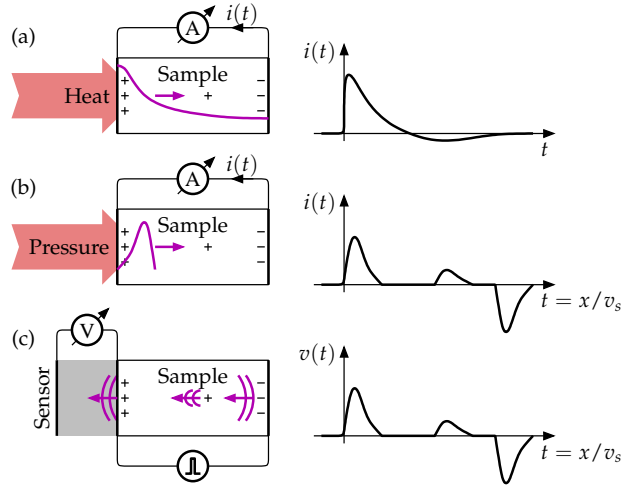
Figure 2: Principle of space charge distribution measurement methods in solids dielectrics. (a) Thermal method: the sample is perturbed by heat which generates an electric signal during the diffusion. Calculations are mandatory to recover the charge distribution from the signal. (b) Pressure-wave-propagation method: the sample is perturbed by a pressure wave which generates an electric signal during the propagation. The signal is a direct image of the charge distribution. (c) Pulsed-electro-acoustic method: the sample is perturbed by a voltage pulse which generates elastic waves that reach a sensor after propagation. The signal is a direct image of the charge distribution. Parameter v_s stands for sound velocity.
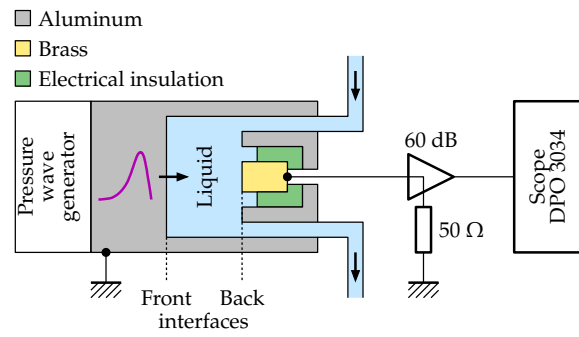
Figure 3: Sketch of the measurement setup. A piezoelectric pressure wave generator produces high amplitude pressure pulses to an aluminum wave-guide that are transmitted into a fluid in direct contact at front side with aluminum and at back side with brass or other materials. The induced electric signal is amplified by a 60-dB amplifier and then digitized by a scope.
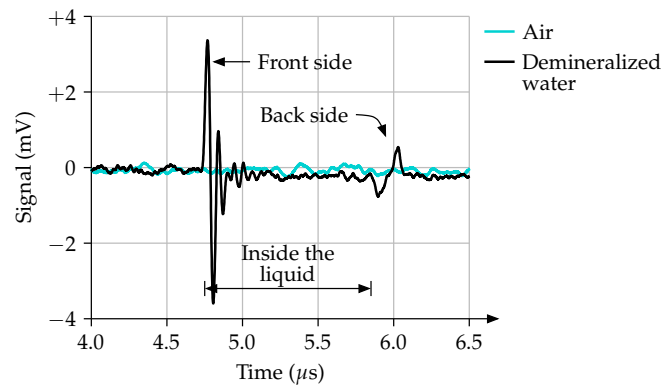
Figure 4: Typical measured signals. Without liquid, no signal is detected. When the liquid enters the measurement setup a clear signal is detected. The front side corresponds to the aluminum/liquid interface and the back side to the liquid/brass interface.
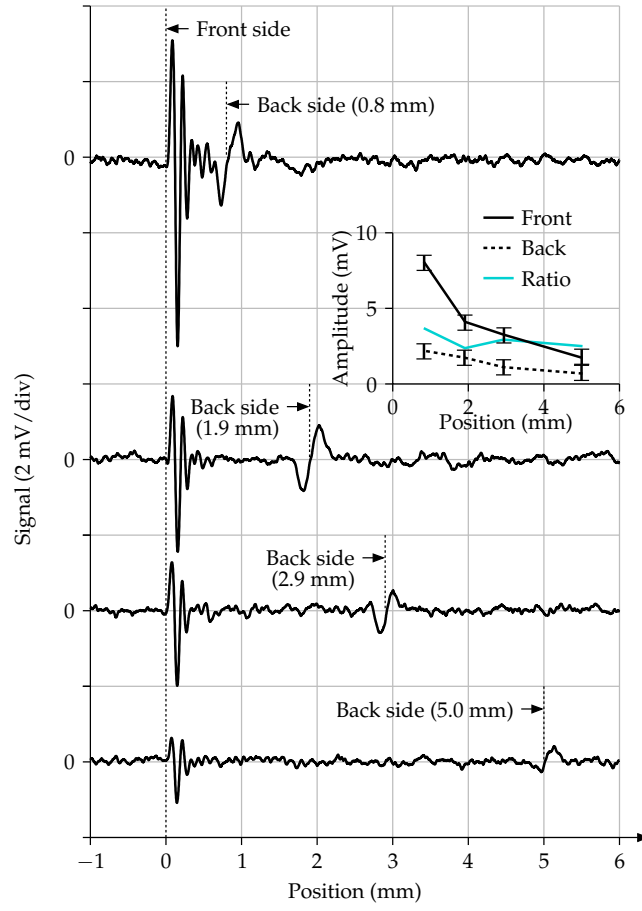
Figure 5: Measured signals with glycerol for various thicknesses. (inset) Peak-to-peak signal amplitude directly depends on the liquid thickness.
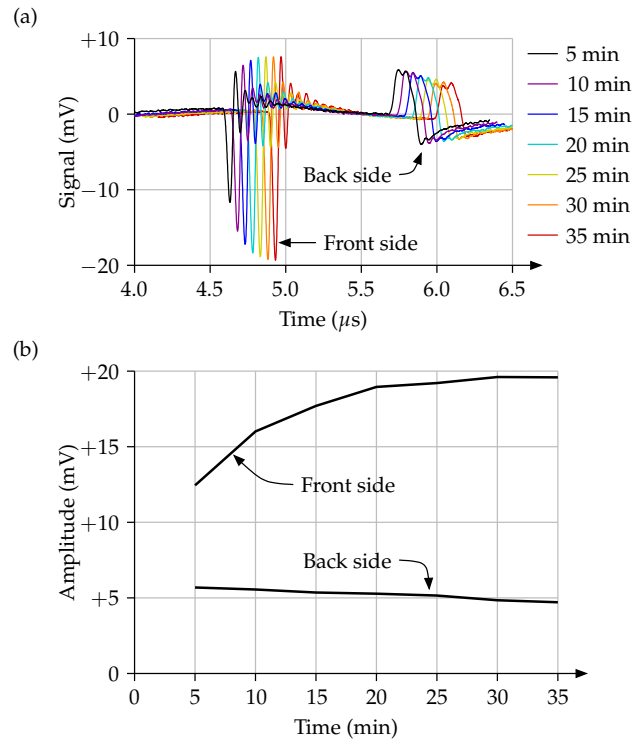
(a)

(b)

Figure 6: (a) Measured signal in salted water (1.25% in weight content) as a function of time. Measured signals have been delayed by 50 ns from one another for clearly seeing the evolution. (b) Signal amplitude corrected from the base line at each interface as a function of time.
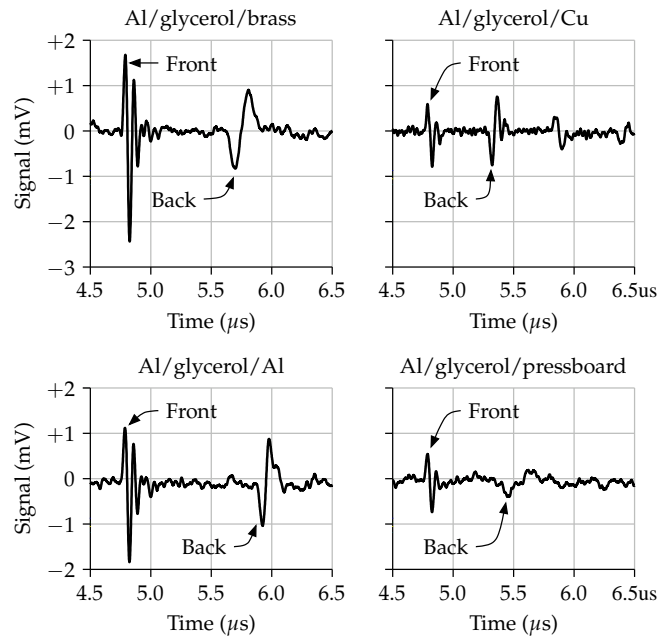
Figure 7: Measured signals with various back interface materials in contact with glycerol.
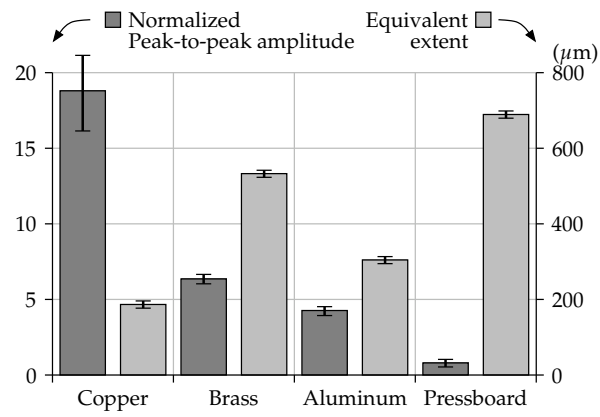
Figure 8: Impedance-corrected peak-to-peak signal amplitude at back side normalized with front side signal amplitude and equivalent extent of back side signal for various materials. Notice that the pressure pulse extends over about 100 μm in glycerol.

Figure 9: Measured signals with various liquid thicknesses and various numbers of averaged acquisitions (indicated above each graph). Only the signal part around the front interface is shown. For 10024 averaged acquisitions, MSO 54 Tektronix scope was used (right) and for 512 averaged acquisitions, DPO 3034 Tektronix scope was used (left).
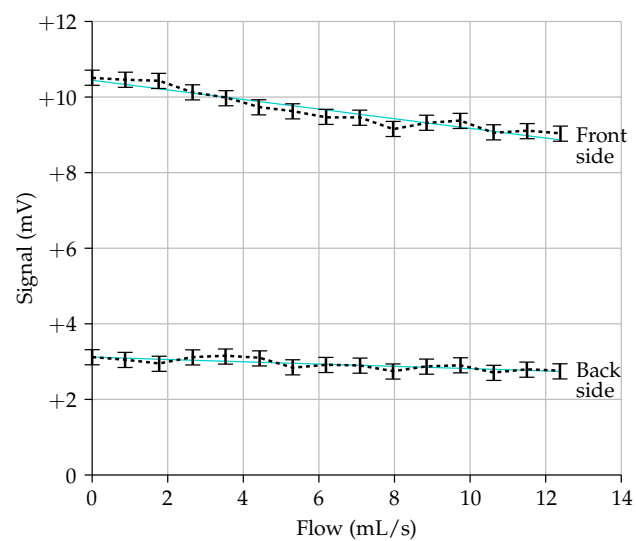
Figure 10: Peak-to-peak signal amplitude at front and back interfaces as a function of glycerol flow rate. Linear regression is indicated with a blue continuous line.
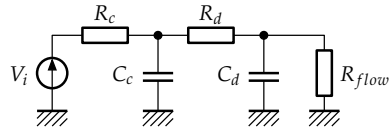
Figure 11: Simplified electric model of the interface. The voltage interface V_i produces charges to the compact layer symbolized by the capacitor C_c. These charges then diffuse to the diffuse layer symbolized by capacitor C_d. The flow directly removes charges from the diffuse layer which can be modeled by a resistor R_{flow}.